Available online at www.sciencedirect.com
ScienceDirect
Journal of the European Ceramic Society 29 (2009) 743–750
www.elsevier.com/locate/jeurceramsoc

Electron irradiation induced rock salt type structure from ZnO/Zn intergrowth

Bang-Hao Huang [a], Pouyan Shen [a], Shuei-Yuan Chen [b,*]

[a] *Institute of Materials Science and Engineering, National Sun Yat-sen University, Kaohsiung, Taiwan, ROC*
[b] *Department of Mechanical and Automation Engineering, I-Shou University, Kaohsiung, Taiwan, ROC*

Received 16 April 2008; received in revised form 12 June 2008; accepted 20 June 2008
Available online 8 August 2008

Abstract

Electron irradiation of nano-size wurtzite (W)-type ZnO condensates with intimate mixture of parallel epitaxial Zn caused $\{1\,0\,\bar{1}\,1\}_W$ slip to form a single domain of rock salt (R)-type core and W-type shell. The two polymorphs follow $(1\,\bar{1}\,1)_R//(0\,\bar{1}\,1\,1)_W$; $[0\,1\,1]_R//[\bar{1}\,2\,\bar{1}\,3]_W$, i.e. chair type Peierls distortion with additional 38° tilting $(0\,0\,1)_R$ along the $(\bar{1}\,2\,\bar{1}\,0)_W$ plane for a fair match of $(1\,0\,\bar{1}\,1)_W/(1\,\bar{1}\,1)_R$, the same as one of the two paths for the back-transformation of R-ZnO into a lower crystal symmetry. The martensitic nucleation of R-type ZnO can be attributed to dynamic migration of interstitials/vacancies, lattice mismatch stress, and capillarity effect.

Keywords: ZnO; Zu; Radiation damage; Crystallography; Electron irradiation; Electron irradiation

1. Introduction

Ambient intrinsic wurtzite (W)-type ZnO, i.e. B4 with Zn in tetrahedral coordination of oxygen, is an n-type semiconductor with a wide direct band gap of 3.37 eV and a high exciton binding energy of 60 meV[1] for applications in the UV region.[2] The denser rock-salt (R)-type ZnO, i.e. B1 structure with Zn in octahedral coordination of oxygen, has an indirect band gap of 2.45 eV at 13.5 GPa[3] and stable above ~10 GPa at room temperature.[4] The B4/B1 phase boundary has a negative $\Delta T/\Delta P$ slope with considerable hysteresis.[5] Size miniature causes significant shift of the phase boundary from 9.9 GPa toward high pressure (15.1 GPa) at ambient temperature according to static compression results.[6]

R-ZnO can be retained to ambient pressure due to a sluggish B1 → B4, i.e. R → W, transformation during static decompression.[7,8] Electron irradiation of such metastable powders has been shown to cause the transformation following preferential $(1\,\bar{1}\,1)_R//(0\,\bar{1}\,1\,1)_W$; $[0\,1\,1]_R//[\bar{1}\,2\,\bar{1}\,3]_W$ and then transformation-strain induced $(1\,1\,\bar{1})_R//(\bar{1}\,0\,1\,1)_W$; $[0\,1\,1]_R//[0\,1\,\bar{1}\,1]_W$.[9] The two relationships can be rationalized by specified extent of so-called chair- and boat-type Peierls distortions, respectively[10] (Appendix 1), accompanied with band gap opening and intermediate $\{1\,1\,1\}_R$ slip for energetically favorable $\{1\,1\,1\}_R/(0\,\bar{1}\,1\,1)_W$ match. In both transition paths, the connectivity of the atoms cannot be altered when viewed as three-dimensional Peierls distortions.[11,12]

Pulsed laser ablation has been used to fabricate W-ZnO condensates with unusual preferred orientation $\{10\bar{1}1\}$ and a significant residual stress due to the combined effects of rapid heating/cooling and thermal/lattice mismatch with respect to co-existing Zn.[13] The residual stress of the W-ZnO and co-existing Zn was estimated to be 2.7 and 5.6 GPa, respectively based on the least squares refinement of the observed d-spacings and the available physical parameters of the Birch-Murnaghan equation of state.[13] Such a stress level is insufficient for the ZnO condensates to form a R-type structure, which is stable above ca. 10 GPa as mentioned.

Here, we report electron-irradiation induced nucleation of the R-type structure from such condensates with W-ZnO/Zn intergrowth focusing on distortion path selection as a comparison of the decompression results.[9] The chair-type distortion turns out to be favorable in the present case of W → R transformation, suggesting that distortion bifurcation can be avoided when a higher crystal symmetry is obtained in the transformation. This knowledge is of importance to understanding the

* Corresponding author.
E-mail address: steven@isu.edu.tw (S.-Y. Chen).

0955-2219/$ – see front matter © 2008 Elsevier Ltd. All rights reserved.
doi:10.1016/j.jeurceramsoc.2008.06.029

compression vs. decompression dependence of chair- and/or boat-type Peierls distortion path for an ionic crystal Electron-irradiation or photon-excitation induced W → R transition of the ZnO/Zn nanocondensates would have potential applications in visible region because of band gap narrowing associated with the phase transformation.

The motivation of this research is to prove experimentally that the epitaxial ZnO/Zn nanocondensates prepared by a dynamic process with significant residual stress can be electron irradiated to form a further dense structure under the influence of dynamic migration of interstitials/vacancies, lattice mismatch stress, and capillarity effect.

2. Experimental

To fabricate condensates, Zn target with negligible impurities (99.9% pure) was subjected to energetic Nd-YAG-laser (Lotis, 1064 nm in wavelength, beam mode: TEM00) pulse irradiation in a chamber pumped to a moderate vacuum of 4×10^{-3} Pa yet with tramp oxygen from target and/or chamber surface. Laser ablation was conducted at 560 mJ/pulse, i.e. power density of 1.17×10^{12} W/cm^2 given pulse time duration of 16 ns at 10 Hz (Q-switch) on a focused area of 0.03 mm^2 for 3 min.

The condensates were collected by copper grids overlaid with a carbon-coated collodion film for field emission transmission electron microscopy (TEM, FEI Tecnai G2 F20 at 200 kV) with selected area electron diffraction (SAED), and point-count energy dispersive X-ray (EDX) analysis at a beam size of 10 nm. EDX analysis of local areas of interest was performed using K shell counts for Zn and O, and the principle of ratio method without absorption correction.[14] Bright field images (BFI) taken by transmission electron microscopy (TEM) were used to study the size and morphology of the as-condensed particles. Lattice imaging coupled with two-dimensional Fourier transform and inverse transform was used to study the phase transformation and lattice mismatch of the individual condensates upon electron irradiation under 200 kV for a prolonged time period up to 60 min. The irradiation time was counted as soon as a fresh sample area was moved in for dynamic electron bombardment with a considerable heating effect.[15] The particles within a specified sample area of 8×10^3 nm^2, a beam diameter of 100 nm, a beam current of 5 nA and hence a beam current density of 6×10^{-4} nAnm^{-2}, were found to suffer W-R-amorphous phase transformation. By contrast, the particles within a much larger selected area of 2×10^7 nm^2 and a relatively low beam current density of 3×10^{-7} nAnm^{-2} using a larger beam diameter of 5 μm and a beam current of 5 nA did not show such phase transformations within a prolonged irradiation time of 3 h. The d-spacings measured from SAED patterns were used for least-squares refinement of the lattice parameters during the process of phase transformation.

3. Results

3.1. As-condensed particles

The as-condensed particles are submicron in size and randomly oriented as indicated by TEM BFI (Fig. 1a) and ring diffractions in the SAED pattern (Fig. 1b). The particles consist of intimate intergrowths of Zn/W-ZnO phases with well developed {1 0 $\bar{1}$ 1} surface of W-ZnO,[13] and have nearly superimposed diffractions of $(0\,0\,0\,2)_{Zn}$ and $(1\,0\,\bar{1}\,1)_{W\text{-}ZnO}$. Point count EDX analysis (Fig. 1c) showed only O and Zn counts with negligible other impurities for such particles. This indicates that tramp oxygen, but not other impurities, was present in

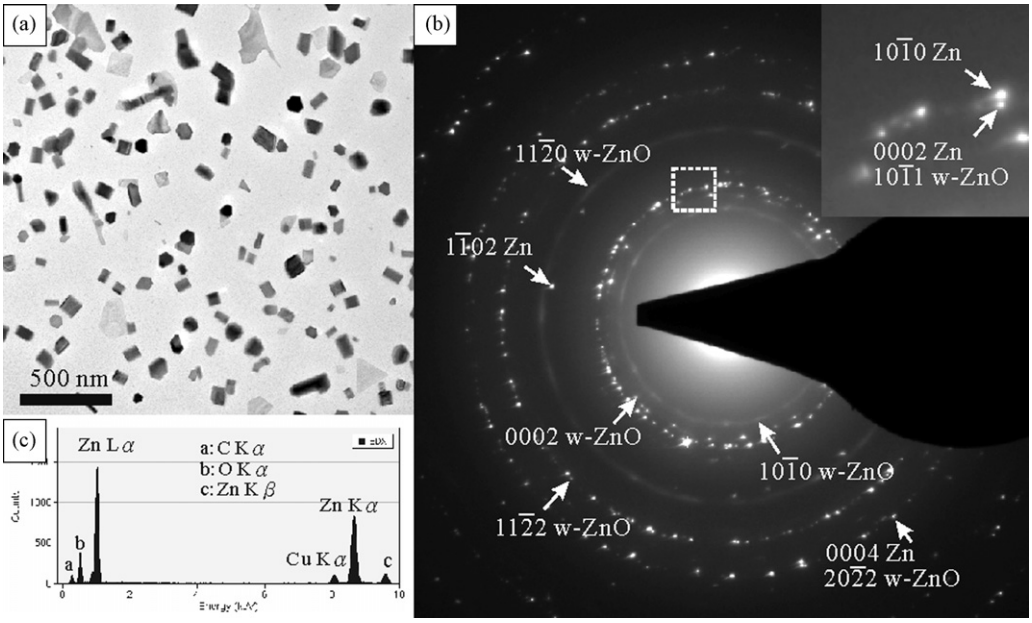

Fig. 1. TEM (a) BFI, (b) SAED pattern with nearly superimposed (0 0 0 2)Zn and $(1\,0\,\bar{1}\,1)_{W\text{-}ZnO}$ magnified as inset, and (c) point count EDX spectrum of randomly oriented Zn/W-ZnO nanocondensates with well developed faces. Sample produced by pulsed Nd-YAG laser ablation on Zn target at 560 mJ pulse energy in vacuum without oxygen flow.

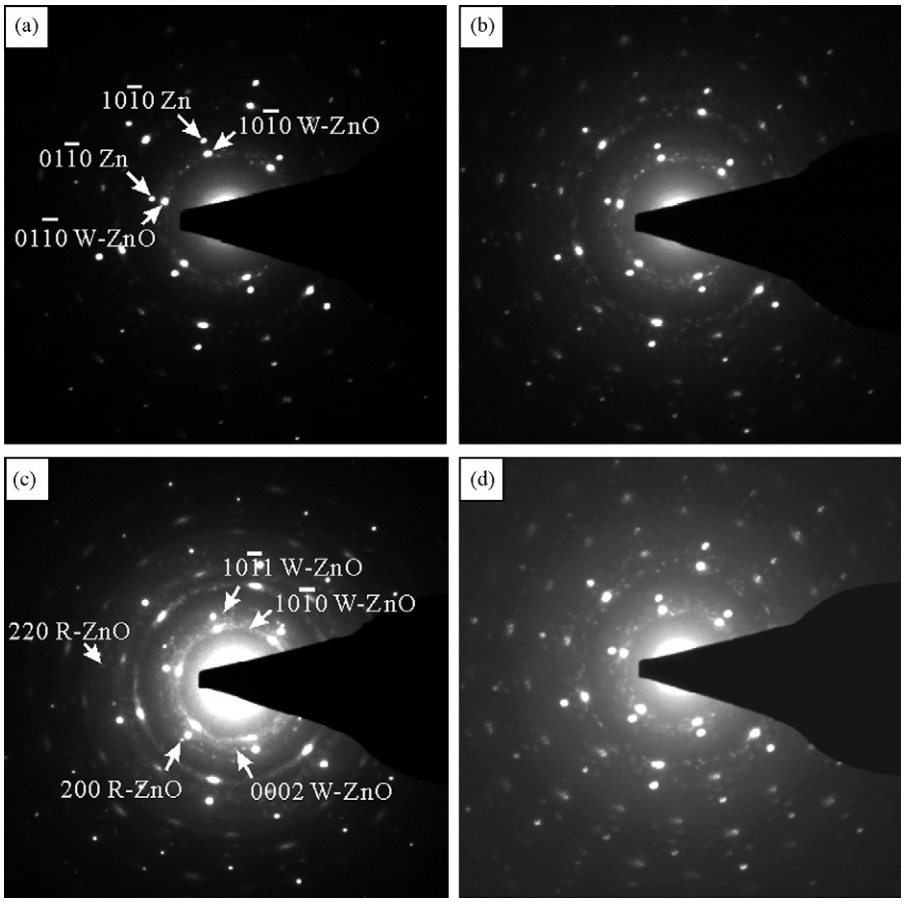

Fig. 2. SAED pattern of a submicron size condensate with intimate mixture of Zn and W-ZnO in [0 0 0 1] zone axis in the same sample as Fig. 1 upon electron irradiation for (a) 1 min (b) 5 min, (c) 15 min and (d) 30 min showing (2 0 0) and (2 2 0) diffractions of R-type ZnO emerged with accompanied relaxation/shuffling of W-ZnO lattice as indicated by broadened (1 0 $\bar{1}$ 0), (0 0 0 2) and (1 0 $\bar{1}$ 1) diffraction rings (as labeled) in (c) and R-ZnO diminishing in (d).

the vacuum chamber and/or target during laser ablation to form the condensates.

3.2. Electron irradiation-induced transformation

The individual condensate up to about 100 nm in size typically showed single crystal diffraction spots and additional ring diffractions due to superimposed nanocondensates when subjected to a rather limited electron dosage (Fig. 2a). Such individual condensates can be unambiguously identified as co-existing Zn and W-ZnO following parallel epitaxial relationship. The structure of the condensate remained unchanged upon electron irradiation for 5 min (Fig. 2b). By contrast, the R-type ZnO with characteristic (2 0 0) and (2 2 0) diffraction spots, having nothing to do with double diffractions, were emerged when subjected to further irradiation up to a total of 15 min. (It is noteworthy that the intimately mixed W-ZnO/Zn condensates have preferred orientation[13] though nanometers in size. This accounts for the strong (2 0 0) and (2 2 0) diffraction spots for the derived R-type phase.) Whereas the diffractions of co-existing W-ZnO became smeared/relaxed, as indicated by broadened (1 0 $\bar{1}$ 0), (0 0 0 2) and (1 0 $\bar{1}$ 1) diffractions spots (Fig. 2c), presumably due to the formation of much denser R-type structure nearby. After a total of 30 min electron dosage, the R-ZnO diffractions disappeared and the W-ZnO remained in [0 0 0 1] zone axis (Fig. 2d). Due to superimposition of some randomly oriented nanocondensates, we failed to determine the epitaxial relationship, if any, between R- and W-ZnO in this case.

The nano-sized condensates containing intimate mixture of Zn and W-ZnO following parallel epitaxial relationship and with abundant misfit dislocations were revealed by lattice image coupled with 2-D forward and inverse Fourier transform in [0 0 0 1] zone axis (Fig. 3) from the same area of the condensate free of artifacts, such as objective astigmatism, in order to study the irradiation time dependence of phase change and the spatial distribution of R-type ZnO. Upon electron irradiation for 20 min (Fig. 3b) the R-type core with Moirè fringes due to superimposition with the W-type shell were developed for ZnO and the orientation changed into $[\bar{1}\,2\,\bar{1}\,3]_W$, i.e. by rotation along $(1\,0\,\bar{1}\,0)_{W\text{-}ZnO}$ plane normal for 32° as discussed later. The resultant R- and W-type ZnO follow chair-type relationship, i.e. $(1\,\bar{1}\,1)_R//(0\,\bar{1}\,1\,1)_W$; $[0\,1\,1]_R//[\bar{1}\,2\,\bar{1}\,3]_W$, with interfacial dislocations having their half planes parallel to $(1\,\bar{1}\,1)_R$ and $(0\,\bar{1}\,1\,1)_W$. The relic Zn remained in [0 0 0 1] zone axis following a secondary crystallographic relationship with W-ZnO, i.e. $(1\,\bar{1}\,0\,1)_W//(0\,1\,\bar{1}\,0)_{Zn}$; $[\bar{1}\,2\,\bar{1}\,3]_W//[0\,0\,0\,1]_{Zn}$ (Fig. 3b) in this case. The core then diminished upon further electron irradiation for a total of 30 min (Fig. 3c). Using the inverse

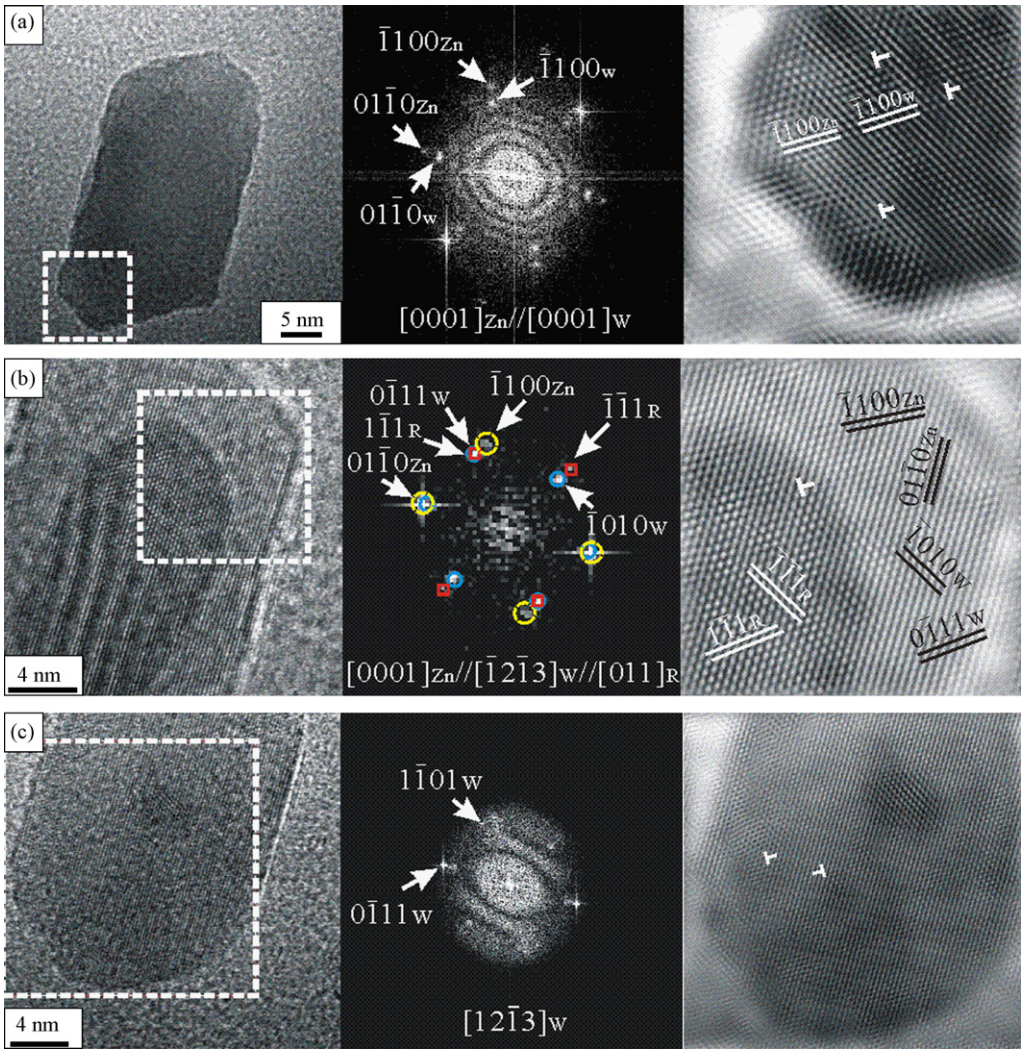

Fig. 3. TEM lattice image (left) and corresponding 2-D forward (middle) and inverse (right) Fourier transform showing the change of the W-ZnO nanocondensate upon electron dosage: (a) as-condensed with intimate mixture of parallel epitaxial yet lattice mismatched Zn in [0 0 0 1] zone axis, (b) forming R-ZnO core and W-ZnO shell with *c*-axis tilted (cf. text) for chair-type epitaxy, i.e. $(1\,\bar{1}\,1)_R//(0\,\bar{1}\,1\,1)_W$; $[0\,1\,1\,]_R//[\bar{1}\,2\,\bar{1}\,3]_W$ upon electron irradiation for 20 min, (c) amorphization of R-ZnO core upon further electron irradiation for a total of 30 min leaving W-ZnO full of dislocations (denoted as T) with half planes parallel to $\{0\,\bar{1}\,1\,1\}$. Note diffractions of Zn, W-ZnO and R-ZnO in (b) are circled in yellow, blue and red, respectively.

Fourier transform, the R-phased diffraction spot was confirmed to come from the core area of the condensates upon suitable electron dosage. The W-ZnO relic has dislocations with half planes parallel to $\{1\,0\,\bar{1}\,1\}$ as shown more clearly in another submicron-sized particle subjected to electron irradiation for a longer time up to 60 min (Fig. 4). Point count EDX spectrum (not shown) of a typical Zn/W-ZnO nanocondensate subjected to electron irradiation for 30 min shows the Zn/O count ratio remained unchanged.

It should be noted that the diffraction spots of R-type ZnO and the R-core/W-shell structure showed only for the intimately mixed W-ZnO/Zn nanocondensates prepared by PLA in vacuum, rather than the pure W-ZnO condensates prepared by the PLA in air, when subjected to the same electron irradiation process. Besides, the electron diffraction spots of R-type ZnO became dimmed when overdosed with electrons. The diffractions of R-type W-ZnO in the present nanocondensates were thus unambiguously determined to depend not only on the ZnO/Zn intergrowths with preferred orientations but also on the suitable electron dosage.

4. Discussion

4.1. Condensation of dense W- rather than R-type ZnO nanoparticles

Extremely rapid heating/cooling via a dynamic laser ablation process for a stress effect was known to generate a number of dense polymorphs for dioxides such as TiO_2[16,17] and SnO_2.[18] The as-condensed ZnO however remained as W-type structure in the similar dynamic laser ablation process because the residual stress is not high enough to trigger W → R transformation as mentioned. The ZnO condensates were likely heated to very high temperatures and cooled to room temperature within the P–T stability field of W-type structure in view of a positive Clauseus-Clayperon slope of the W/R phase boundary for the

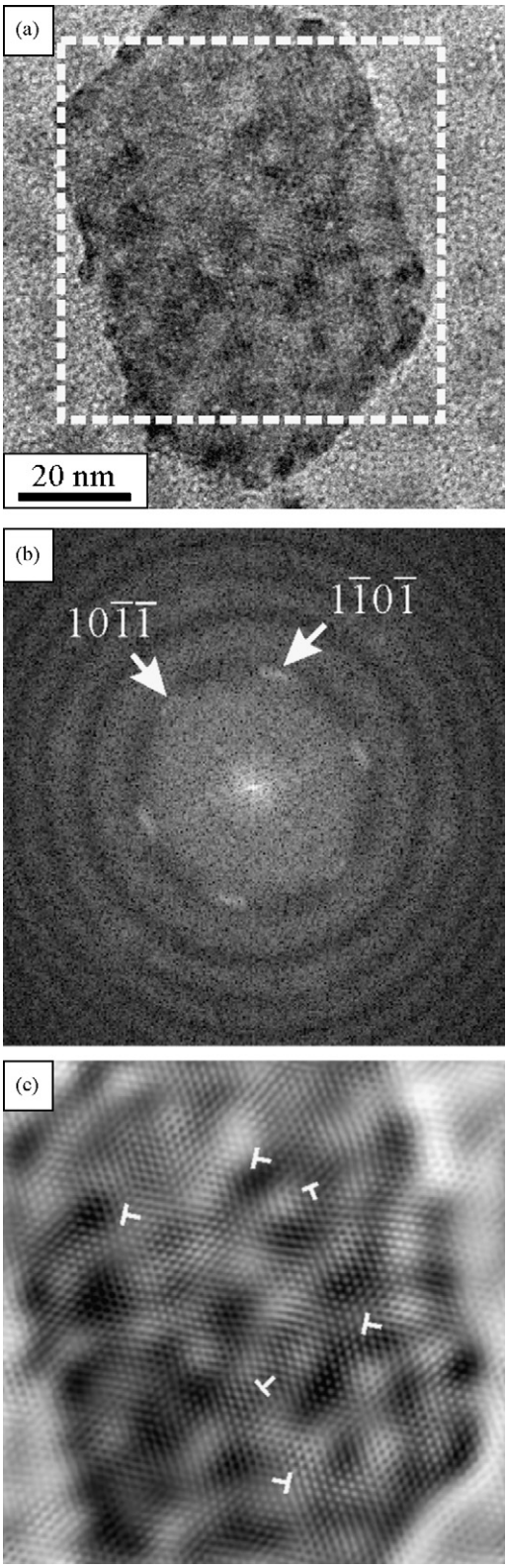

Fig. 4. (a) Lattice image of a submicron size particle subjected to electron irradiation for 60 min, (b) and (c) 2-D forward and inverse Fourier transform, respectively of the square region in (a) showing more clearly dislocations (denoted as T) with half planes parallel to $\{10\bar{1}1\}$ of W-ZnO.

bulk[4] and nanocrystals,[6] although the possible effect of oxygen partial pressure on the phase boundary is not clear.

4.2. Bulk nucleation of R-ZnO from W-ZnO/Zn nanocondensates

The R-type structure always emerged at the center rather than the surface of the nanocondensates with intimate mixture of W-ZnO and Zn, indicating that surface energy is of minor importance than elastic strain energy on the nucleation event. The individual nanocondensate likely has the highest stress at its center for the nucleation of R-ZnO upon electron irradiation, analogous to so called carbon onion pressure cell to form diamond in the core.[19] The R-ZnO core was likely surrounded by $Zn_{1+x}O$ shell, although EDX is difficult, if not impossible, to detect the extent of nonstoichiometry x. In fact, the negatively charged Zn interstitials in coordination 4 and charge compensating oxygen as well as Zn-on-O antisite, are pertinent to n-type W-ZnO.[20] We believe that electron irradiation induced an outward diffusion of Zn in vacuum and the dynamics of migration of interstitials/vacancies would cause the contraction of the whole particle as in the case of graphite to diamond transformation.[21]

In addition, there is a significant lattice mismatch from ca. 18% for $(1\,0\,\bar{1}\,0)_{Zn}/(1\,0\,\bar{1}\,0)_{W}$ or $(1\,1\,\bar{2}\,0)_{Zn}/(1\,1\,\bar{2}\,0)_{W}$ of primary parallel epitaxial relationship (Fig. 3a) down to ca. 3% for $(0\,0\,0\,1)_{Zn}/(1\,0\,\bar{1}\,1)_{W}$ of a secondary relationship (Fig. 3b) as compiled in Table 1. It is reasonable that a relatively high lattice misfit stress for the primary than secondary epitaxial relationship would help nucleate the R-type structure with accompanied orientation change of W-ZnO for beneficial lower strain energy among Zn, W- and R-type ZnO. (The change in crystallographic relationship of W-ZnO with respect to Zn can be accounted for by $\{0\,1\,\bar{1}\,\bar{1}\}_{W}$ slip, i.e. apparent tilting along $(1\,0\,\bar{1}\,0)_{W}$ plane normal for 32° as shown in the stereogram of ref.[13])

Furthermore, an optimal small size of the nanocondensate may exert significant capillarity force at the glissile core-shell interface in such a displacive transformation. The deviatoric shear stress due to electron dosage could also be effective for the formation of R-type structure at the expense of relaxed/faulted W-ZnO in view of electron-irradiation[22] or ball-milling[23] induced high-pressure phase change of TiO_2, and the

Table 1
Lattice misfit for the adjoined $(h\,k\,i\,l)_{Zn}/(h\,k\,i\,l)_{W}/(h\,k\,l)_{R}$

Lattice Plane	d spacing (nm)	Misfit (%)	Remark
$(0\,0\,0\,1)_{Zn}/(0\,0\,0\,1)_{W}$	0.476/0.516	7.7	Fig. 3a
$(1\,0\,\bar{1}\,0)_{Zn}/(1\,0\,\bar{1}\,0)_{W}$	0.226/0.275	17.8	Fig. 3a
$(1\,1\,\bar{2}\,0)_{Zn}/(1\,1\,\bar{2}\,0)_{W}$	0.130/0.161	19.2	Fig. 3a
$(0\,0\,0\,2)_{Zn}/(1\,0\,\bar{1}\,1)_{W}$	0.239/0.246	2.8	Fig. 3b
$(1\,\bar{1}\,0\,0)_{Zn}/(1\,0\,1\,1)_{W}$	0.227/0.246	7.7	Fig. 3b
$(1\,0\,\bar{1}\,1)_{W}/(1\,\bar{1}\,1)_{R}$	0.246/0.246	<0.1	Fig. 3b

Note Fig. 3a and b refer to primary and secondary epitaxial relationship, respectively (cf. text). The cell parameters $a = 0.427$ nm for R-ZnO; $a = 0.321$ nm, $c = 0.512$ nm for W-ZnO; and $a = 0.262$ nm, $c = 0.476$ nm for Zn are based on least-squares refinement of the d-spacings measured from ring electron diffractions.

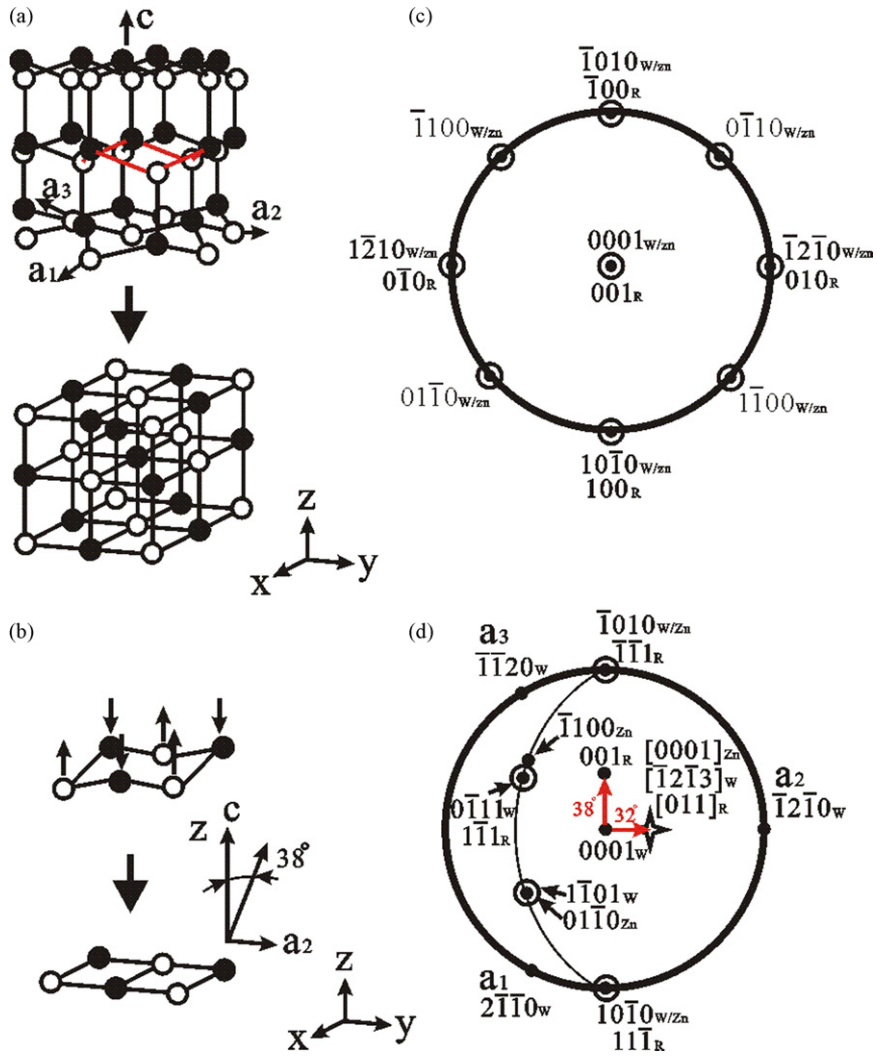

Fig. 5. (a) Wurtzite and rock salt structure, with anions and cations denoted by open and solid circles, respectively. The "chair" type structure is highlighted in the wurtzite lattice. (b) Schematic drawing showing a six membered ring "chair" type structure in a wurtzite (0 0 0 1) plane becomes a 2×3 rectangle in a rock salt (0 0 1) plane. Additional 38° tilting $(0\,0\,1)_R$ along the $(\bar{1}\,2\,\bar{1}\,0)_W$ plane is required for the crystallographic relationship specified in (d) with accompanied tilting along $(1\,0\,\bar{1}\,0)_W$ plane normal by 32° for a fair match with $(1\,0\,\bar{1}\,0)_{Zn}$ as denoted by arrows in orthogonal directions (cf. text). (c) and (d) are corresponding stereograph projections of (a) and (b) constructed with $c/a = 1.602$ for W-ZnO at ambient pressure[24,25] showing the deviation from ideal case of $(0\,0\,1)_R//(0\,0\,0\,1)_W$; $(0\,1\,0)_R//(\bar{1}\,2\,\bar{1}\,0)_W$ (c) into (d) was achieved by tilting $(0\,0\,1)_R$ along the $(1\,0\,0)_R$, i.e. $(1\,0\,\bar{1}\,0)_W$ for specified crystallographic relationship. Open and solid circles denote R and W plane normal, respectively, whereas star denotes direction. The plane normals of co-existing Zn are also specified.

effect of an applied shear stress on the olivine-spinel transformation for $(Fe,Mg)_2SiO_4$ silicates.[24]

4.3. Peierls distortion path selection

The present crystallographic relationships for W → R transformation belongs to chair-type Peierls distortion with additional 38° tilting $(0\,0\,1)_R$ along the $(\bar{1}\,2\,\bar{1}\,0)_W$ plane and accompanied tilting along $(1\,0\,\bar{1}\,0)_W$ plane normal by 32° for a fair match with $(1\,0\,\bar{1}\,0)_{Zn}$, as shown by the stereographic projection (Fig. 5) constructed with the ambient c/a ratio of W-ZnO.[25,26] (Note it was mistaken as an additional 13° tilting $(0\,0\,1)_R$ along the $(1\,0\,\bar{1}\,0)_W$ plane for the same chair-type Peierls distortion, although R → W rather than W → R transformation in ref.[9]). The fair match of $(1\,0\,\bar{1}\,1)_W/(1\,\bar{1}\,1)_R$ is the same as one of the two paths reported for the back-transformation of R-ZnO.[9] In other words, atom connectivity and a single Peierls distortion path are valid for the W → R transformation toward a higher crystal symmetry. Such a martensitic/displacive transformation involves $\{1\,0\,\bar{1}\,1\}_W$ slip rather than twinning to form a single domain of R-type core despite rather complicated anisotropic lattice misfit for the adjoined $(h\,k\,l)_R$, $(h\,k\,i\,l)_W$ and $(h\,k\,i\,l)_{Zn}$ planes as compiled in Table 1.

The prevailing chair-type distortion path for the present B4 → B1 transformation is about the distortion of a hexagon of three MX molecules in a chair conformation to form a planar pattern of 3×2 rectangles. This is different from a boat → 3×2 B1 face route for B4 → B1 transformation according to constant-stress molecular dynamic simulation of a model ionic system.[27] A fair match of $(1\,0\,\bar{1}\,1)_W/(1\,\bar{1}\,1)_R$, a significant surface energy effect, and a rather complicated lattice misfit as mentioned would account for the distortion path for the present nanocondensates.

It is not clear if the transformation kinetics, in terms of activation energy and activation volume as the case of solid-solid transformations of CdSe nanocrystals,[28] would affect the distortion path of the present B4 → B1 transformation.

4.4. Implications

The W → R transformation of the present ZnO/Zn nanocondensates upon electron irradiation or photon excitation may have potential applications in visible region because of band gap narrowing as a result of Zn coordination change from 4 to 6.[1–3] On the other hand, amorphization of ZnO would cause Zn^{2+} to be in tetrahedral site in view of vibrational spectroscopic results of analogous material, i.e. Zn_2SiO_4 gel.[29] Thus, a stepwise W → R → amorphous phase transition upon prolonged electron/photon dosage would exert a time constraint for such applications.

5. Conclusions

1. Electron irradiation of nano-sized condensates with intimate intergrowth of W-ZnO/Zn caused $\{1\,0\,\bar{1}\,1\}_W$ slip to form a R-type core following $(1\,\bar{1}\,1)_R//(0\,\bar{1}\,1\,1)_W$; $[0\,1\,1]_R//[\bar{1}\,2\,\bar{1}\,3]_W$, i.e. chair Peierls distortion relationship, with the W-type shell of ZnO.
2. The W → R transformation of ZnO was near completion within 20 min upon electron dosage at a specific electron current density.
3. The nucleation of a R-type structure in the core of the condensates can be rationalized by lattice mismatch, capillarity effect, and the migration of interstitial/vacancies upon electron dosage.

Acknowledgments

We thank C.N. Huang for technical assistance on laser ablation and L.J. Wang for technical assistance on AEM. Supported by Center for Nanoscience and Nanotechnology at NSYSU and National Science Council, Taiwan, ROC under contract NSC95–2221-E-214–040.

Appendix A. Appendix 1

Peierls distortion paths for the R → W type transformation of ZnO

Peierls distortion path was recently proved experimentally for dense R-ZnO nanoparticles prepared by static compression.[9] Electron irradiation was found to cause R to W transition, following preferential $(1\,\bar{1}\,1)_R//(0\,\bar{1}\,1\,1)_W$; $[0\,1\,1]_R//[\bar{1}\,2\,\bar{1}\,3]_W$ and then transformation strain induced $(1\,1\,\bar{1})_R//(\bar{1}\,0\,1\,1)_W$; $[0\,1\,1]_R//[0\,1\,\bar{1}\,1]_W$. The two relationships were rationalized by specific extent of chair- and boat-type Peierls distortion accompanied with band gap opening and intermediate $\{1\,1\,1\}_R$ and/or $\{\bar{1}\,0\,1\,1\}_W$ slip for energetically favorable $\{1\,1\,1\}_R$ and/or $\{\bar{1}\,0\,1\,1\}_W$ match. Theoretically, chair-type Peierls distortion is about puckering of (0 0 1)R plane to become $(0\,0\,0\,1)_W$ plane, whereas boat-type Peierls distortion refers to puckering of $(0\,1\,0)_R$ plane to become $(\bar{1}\,2\,\bar{1}\,0)_W$ plane.[10] The observed crystallographic relationships as compiled in the stereograms of ref.[9] should be corrected as that $[0\,0\,1]_R$ originally aligned with $[0\,0\,0\,1]_W$ became tilted for ca. 38° and 4.6° along the plane $(\bar{1}\,2\,\bar{1}\,0)_W$ (cf. Fig. 5d of this work) and $(2\,\bar{1}\,\bar{1}\,0)_W$, for the chair- and boat-type distortions, respectively. The specific Peierls distortion was also rationalized by anisotropic lattice mismatch strain for the adjoined $(h\,k\,l)_R$ and $(h\,k\,i\,l)_W$ planes based on lattice parameters of the polymorphs at various pressures.[9]

References

1. Hvam, J. M., Optical gain and induced absorption from excitonic molecules in ZnO. *Solid State Commun.*, 1978, **26**, 987–990.
2. Kollias, N., The absorption properties of "Physical" sunscreens. *Arch. Dermatol.*, 1999, **135**, 209.
3. Sequra, A., Sans, J. A., Manjón, F. J., Muñoz, A. and Herrera-Cabrera, M. J., Optical properties and electronic structure of rock-salt ZnO under pressure. *App. Phys. Lett.*, 2003, **83**, 278–280.
4. Bates, C. H., White, W. B. and Roy, R., New high-pressure polymorph of zinc oxide. *Science*, 1962, **137**, 993.
5. Decremps, F., Zhang, J. and Liebermann, R. C., New phase boundary and high-pressure thermoelasticity of ZnO. *Europhys. Lett.*, 2000, **51**, 268–274.
6. Jiang, J. Z., Olsen, J. S., Gerward, L., Frost, D., Rubie, D. and Peyronneau, Structural stability in nanocrystalline ZnO. *J. Europhys. Lett.*, 2000, **50**, 48–53.
7. Decremps, F., Pellicer-Porres, J., Datchi, F. J., Itie, J. P., Polin, A., Baudelet, F. *et al.*, Trapping of cubic ZnO nanocrystallites at ambient conditions. *App. Phys. Lett.*, 2002, **81**, 4820–4822.
8. Mujica, A., Rubio, A., Munoz, A. and Needs, R. J., High-pressure phases of group-IV, III–V, and II–VI compounds. *Rev. Mod. Phys.*, 2003, **75**, 863–912.
9. Chen, S. Y., Shen, P. and Jiang, J. Z., Polymorphic transformation of dense ZnO nanoparticles: implications for chair/boat-type Peierls distortions of AB semiconductor. *J. Chem. Phys.*, 2004, **121**, 11309–11313.
10. Tolbert, S. H. and Alivisatos, A. P., The wurtzite to rock salt structural transformation in CdSe nanocrystals under high pressure. *J. Chem. Phys.*, 1995, **102**, 4642–4656.
11. Burdett, J. K. and McLarnan, T. J., A study of the arsenic, black phosphorus, and other structures derived from rock salt by bond-breaking processes. I. Structural enumeration. *J. Chem. Phys.*, 1981, **75**, 5764–5775.
12. Burdett, J. K., From bonds to bands and molecules to solids. *Prog. Solid State Chem.*, 1984, **15**, 173–255.
13. Huang, B. H., Shen, P. and Chen, S. Y., {1 0 $\bar{1}$ 1} Artificial epitaxy of ZnO on glass via pulse laser deposition. *J. Euro Ceram. Soc.*, 2008, **28**, 2545–2555.
14. Williams, D. B., *Practical Analytical Electron Microscopy in Materials Science*. Philips Electronic Instruments Inc., Mahwah, 1984.
15. Meldrum, A., Wang, L. M. and Ewing, R. C., Electron-beam-induced crystallization and phase segregation in crystalline and amorphous apatite: a TEM study. *Am. Mineral.*, 1997, **82**, 858–869.
16. Chen, S. Y. and Shen, P., Laser ablation condensation of α-PbO_2-type TiO_2. *Phys. Rev. Lett.*, 2002, **89**, 096106-1–096106-4.
17. Chen, S. Y. and Shen, P., Laser ablation condensation and transformation of baddeleyite-type related TiO_2. *Jpn. J. App. Phys.*, 2004, **43**, 1519–1524.
18. Tseng, W. J., Shen, P. and Chen, S. Y., Defect generation of rutile-type SnO_2 nanocondensates: imperfect oriented attachment and phase transformation. *J. Solid State Chem.*, 2006, **179**, 1237–1246.
19. Banhart, F. and Ajayan, P. M., Carbon onions as nanoscopic pressure cells for diamond formation. *Nature*, 1996, **382**, 433–435.
20. Özgür, Ü., Alivov, Y. I., Liu, C., Teke, A., Reshchikov, M. A., Doğan, S. *et al.*, A comprehensive review of ZnO materials and devices. *J. App. Phys.*, 2005, **98**, 041301-1–041301-103.
21. Bar-Yam, Y. and Moustakas, T. D., Defect-induced stabilization of diamond films. *Nature*, 1989, **342**, 786–787.
22. Shen, P., Hwang, S. L., Chu, H. T., Yui, T. F., Pan, C. and Huang, W. L., On the transformation pathways of α-PbO_2-type TiO_2 at the twin boundary of

rutile bicrystals and the origin of rutile bicrystals. *European J. Mineralogy*, 2005, **17**, 543–552.
23. Begin-Colin, S., Caer, G. Le, Mocellin, A. and Zandona, M., Polymorphic transformations of titania induced by ball milling. *Phil. Mag. Lett.*, 1994, **69**, 1–7.
24. Wu, T. C., Bassett, W. A., Burnley, P. C. and Weathers, M. S., Shear-promoted phase transitions in Fe_2SiO_4 and Mg_2SiO_4 and mechanism of deep earthquakes. *J. Geophy. Res. B*, 1993, **98**, 19767–19776.
25. Abrahams, S. C. and Bernstein, J. L., Remeasurement of the structure of hexagonal ZnO. *Acta Cryst. B*, 1969, **25**, 1233–1236.
26. Hyde, B. G. and Andersson, S., *Inorganic Crystal Structures*. John Wiley & Sons, 1989.
27. Wilson, M. and Madden, P. A., Transformations between tetrahedrally and octahedrally coordinated crystals: the wurtzite → rocksalt and blende → rocksalt mechanisms. *J. Phys. Condens. Mater.*, 2002, **14**, 4629–4643.
28. Jacobs, K., Zaziski, D., Scher, E. C., Herhold, A. B. and Alivisatos, A. P., Activation volumes for solid-solid transformations in nanocrystals. *Science*, 2001, **293**, 1803–1806.
29. Lin, C. C. and Shen, P., Sol–gel synthesis of zinc orthosilicate. *J. Non-cryst. Solids*, 1994, **171**, 281–289.